Egypt. J. Chem. **Vol. 68**, No. 4 pp. 271 - 284 (2025)

Egyptian Journal of Chemistry

http://ejchem.journals.ekb.eg/

Design, Sequential Synthesis, Kinase Inhibitors Comparative Docking, MD Simulations, ^{99m}Tc-Coupling and In-Vivo Studies of Novel Pyrazolopyrimidine Derivatives

Wafaa Zaghary[a], Dina Adel[b], Basma M Essa[c], Tamer Nasr[d,a], Khaled El-Adl[e,f,*], Tamer M Sakr[c]

[a] *Department of Pharmaceutical Chemistry, Faculty of Pharmacy, Helwan University, Egypt.*

[b] *Pharmaceutical Chemistry Department, Faculty of Pharmacy, MSA University, Cairo, Egypt.*

[c] *Radioactive Isotopes and Generator Department, Hot Labs Center, Egyptian Atomic Energy Authority, 13759, Cairo, Egypt*

[d] *Department of Pharmaceutical Chemistry, Faculty of Pharmacy, Modern University for Technology and Information, Egypt.*

[e] *Pharmaceutical Chemistry Department, Faculty of Pharmacy, Heliopolis University for Sustainable Development, Cairo, Egypt.*

[f] *Pharmaceutical Chemistry Department, Faculty of Pharmacy, Al-Azhar University, Cairo, Egypt*

Abstract

Pyrazolopyrimidine derivative was synthesized and labeled with ^{99m}Tc using sodium dithionite as reducing agents. The purity of radiochemical ^{99m}Tc($Na_2S_2O_4$)-compound was 93.4%, and the synthesized complex was stable *in vitro* for 6 hours. Furthermore, using a radiolabeling technique, a bio-distribution investigation showed that tumor-bearing mice exhibited a remarkable absorption of [^{99m}Tc]Tc-complex, with a significant concentration in tumor tissues and a T/NT of 6.58 after 60 minutes after injection. These encouraging results mean that the synthesized compound offers a potential radio-carrier that can be used as a tumor marker and, following additional preclinical research, can be used for cancer therapy. Molecular dynamic simulation confirmed the stability of this compound in the active sites of both EGFR and VEGFR-2 receptors.

Keywords: Pyrazolopyrimidines, Comparative docking, Kinase inhibitors, ^{99m}Tc-coupling, Tumor imaging; MD simulation.

1. Introduction

Cancer, one of the main reasons of death, is a complex, flexible, and heterogeneous result of genetic alterations that perturb cells' regular behavior and function [1,2]. Despite substantial improvements in treatment, researchers still face obstacles such medication resistance, severe side effects, and mutations [3]. WHO estimates that 10 million people died from cancer in 2020, with breast cancer, rectal, colon, skin, prostate, and stomach cancer having the greatest impact [4]. The term targeted cancer therapies refers to the development of new medications that could inhibit a particular target protein or enzyme for treatment of many different types of tumors [5,6]. The proto-oncogene tyrosine protein kinase sarcoma (SCR), platelet-derived growth factor,

*Corresponding author e-mail: eladlkhaled74@yahoo.com ; eladlkhaled74@azhar.edu.eg ;(Khaled El-Adl)
Receive Date: 09 July 2024, Revise Date: 29 August 2024, Accept Date: 29 August 2024
DOI: 10.21608/ejchem.2024.302958.9979

vascular endothelial growth factor receptor (VEGFR), and epidermal growth factor receptor (EGFR) families are among the most important groups of tyrosine kinases (TKIs). One molecular targeted therapy that is being rapidly researched for a variety of cancer types is TKIs [7,8]. ABL-Kinase, Abl-c Kinase, EGFR, VEGFR, and Serine-Threonine Protein Kinase B-Raf (BRAF) are among the main oncogenic therapeutic targets, according to the current drug discovery curve. In order to acquire nutrients and oxygen, the adjacent cells help the cancer; they also aid in the formation of new blood vessels. The lymphatic and blood vascular networks allow it to spread to other organs, including the lung, bones and liver [9-12]. Tumor growth, angiogenesis, and metastasis can be stopped by suppressing the expression of the epidermal growth factor receptor (EGFR) and the vascular endothelial growth factor receptor (VEGFR-2) [13,14].

The two signaling pathways are comparable. VEGF expression is decreased when EGFR is blocked, along with angiogenesis, and VEGFR-2 gradually increases to a resistance level that is comparable to EGFR inhibitors [15]. VEGF is more important to EGFR-mutant malignancies than it is to EGFR wild-type tumors [16]. Nearly ninety percent of EGFR-mutant NSCLC cancers had either exon 19 deletions or exon 21 L858R mutations, which cause tumors to be sensitive to EGFR TKIs [17]. EGFRTKIs have become standard first-line treatment in the metastatic scenario cause of their high tolerability and efficacy for progression-free survival (PFS) [18]. By working together to target and treat cancer cells, concurrent inhibition of EGFR and VEGFR-2 has proven helpful [19]. An ATP binding site found on both enzymes facilitates the efficient binding of certain small molecules that function as dual inhibitors such as Erlotinib (I), gefitinib (II), sorafenib (III), vandetanib (IV), lapatinib (V), and afatinib (VI) [20].

Radiopharmaceutical therapy (RPT) as a new therapeutic treatment procedure for cancer interested a great degree of commercial and recognition attention [21]. Compounds and biomolecules are radiolabeled with non-metallic or metallic radionuclides with the required radiation sort and half-lives for the proposed use. Imaging medications are being used regularly in oncology, neurology, and cardiology, etc. Their development and design is a moderately interdisciplinary procedure covers numerous types of science: regulatory, engineering, medicine, analytical, pharmaceutical, radiochemistry, chemistry, etc. The usage of radionuclides was described some time ago for therapeutic applications. Many malignant and benign tumors have been treated effectively by using numerous radionuclides. Such as, numerous novel radiopharmaceuticals and radionuclides have been established for treating neuroendocrine and metastatic bone pain and other non-malignant or malignant tumors [22].

2. Material and Methods

Materials Sigma-Aldrich (Cairo, Egypt) provided the analytical grade chemicals. The National Cancer Institute (Dokki, Egypt) supplied 20–25 g Female Swiss Albino mice. Technetium-99m was eluted as $^{99m}TcO4$- (activity: 1Ci, Radioisotope Production Facility, Cairo, Egypt) from a $^{99Mo/99m}Tc$ generator. All animal experiments comply with the ARRIVE guidelines and were carried out in accordance with the U.K. Animals (Scientific Procedures) Act, 1986 and associated guidelines, EU Directive 2010/63/EU for animal experiments. Molecular Docking of Pyrazolopyrimidine: The Protein Data Bank's 4ASD code allowed users to download the crystal structure of GSK3b in complex with the inhibitor. Using the X-ray diffraction method, it was produced with an R-value of 0.226 and a resolution of 2.6 Å. Every interaction with Thr201, Gln240, Asp248, Asp244, Lys257, Asp174, Asp107, and Lys266 that is conserved were noted, and all coordinates were obtained from the pdb. In the molecular docking studies, AutoDock Tools [23] and Molsoft softwares [24] were used. The protein was handled with the Amber 18 molecular dynamics simulations package [25] using the AMBERff14SB force field [26], while the ligands were assigned the GAFF2 force field [27].

2.1. General Chemistry

Using the outlined procedures [28-30], the following precursors and intermediary compounds were produced: 4-chloro-1-phenyl-1*H*-pyrazolo[3,4-d]pyrimidine (4), 1-phenyl-1,5-dihydro-4*H*-pyrazolo[3,4-d]pyrimidin-4-one (3), ethyl 5-amino-1-phenyl-1*H*-pyrazole-4-carboxylate (2) and ethyl 2-cyano-3-ethoxyacrylate (1). Mass spectra (MS) were performed at 70 e.v by GCMS-QP1000

EX spectrometer using the Electron Ionization Technique (EI) at the Regional Center for Mycology and Biotechnology, Al-Azhar University, Cairo, Egypt. Infrared spectra were recorded on a Schimadzu FT-IR Affinity-1 Spectrometer, Infrared spectrometer at cm^{-1} scale using KBr disc technique at Faculty of Pharmacy - MSA University, Egypt .NMR Spectra were recorded on Mercury spectrometer at 300 MHz or Bruker at faculty of Pharmacy; Ain Shams University, Cairo, Egypt. TLC technique is used to follow reactions. Ethanol was used for crystallization to create each material, and the DMSO-d6 solvent was used to produce the ^{1}H NMR and ^{13}C NMR spectra at 400 MHz and 100 MHz, respectively.

2.1.1. General procedure for synthesis of ethyl 2-cyano-3-ethoxyacrylate (1)

In the presence of acetic anhydride (26 gm, 0.2 mole), triethylorthoformate (14.8 gm, 0.1 mole) and ethyl 2-cyanoacetate (11.3 gm, 0.1 mole) reacted. Following a five-hour reflux period, the mixture was submerged in iced water to form ethyl 2-cyano-3-ethoxyacrylate precipitate (1). Yield= 85 % as reported; M.P= 50-52 °C as recorded.

2.1.2. *General procedure for synthesis ethyl 5-amino-1-phenyl-1H-pyrazole-4-carboxylate (2)*

For four hours, 10 milliliters of phenylhydrazine was heated under reflux with (16.9 gram, 0.1 mole) of ethyl 2-cyano-3-ethoxyacrylate in 100 milliliters of ethanol. After the mixture was cooled, ethyl 5-amino-1-phenyl-1*H*-pyrazole-4-carboxylate was precipitated by adding it to ice water. Yield and M.P = 80% and 98–100 °C as recorded respectively.

2.1.3. General method for synthesis of 1-phenyl-1,5-dihydro-4H-pyrazolo[3,4-d]pyrimidin-4-one (3)

Refluxing for six hours of a mixture of formamide (50 ml) and ethyl 5-amino-1-phenyl-1*H*-pyrazole-4-carboxylate (23.1 gm, 0.1 mole). After cooling and being poured onto ice-filled water, the obtained precipitate was filtered to obtain 1-phenyl-1,5-dihydro-4*H*-pyrazolo[3,4-d]pyrimidin-4-one (3).

Yield, 80%; m.p. 300–2 °C; ^{1}H NMR (400 MHz, DMSO-d6): 12.43 (s, 1H, NH, D_2O exchangeable), 8.33 (s, 1H, CH of pyrimidine), 8.20 (s, 1H, CH of pyrazole), 8.03–8.05 (d, 2H, H-2, H-6 of C_6H_5), 7.56–7.58 (m, 2H, H-3, H-5 of C_6H_5), 7.38–7.42 (m, 1H, H-4 of C_6H_5).

2.1.4. General method for 4-chloro-1-phenyl-1H-pyrazolo[3,4-d]pyrimidine synthesis (4)

For 12 hours, a mixture of 1-phenyl-1,5-dihydro-4H-pyrazolo[3,4-d]pyrimidin-4-one (3) (21.2 g, 0.1 mol) was refluxed in phosphorous oxychloride (100 ml) in the presence of DMF (20 ml). The reaction mixture was poured onto ice-water to precipitate 4-chloro-1-phenyl-1*H*-pyrazolo[3,4-d] pyrimidine (4) after allowing it to cool to room temperature.

Yield, 70%; m.p. 160–2 °C; ^{1}H NMR (400 MHz, DMSO-d6): 8.14–8.16 (d, 4H, H-2, H-6 of C_6H_5, CH of pyrazole, CH of pyrimidine), 7.50–7.54 (m, 2H, H-3, H-5 of C_6H_5), 7.30–7.34 (m, 1H, H-4 of C_6H_5),

2.1.5. General method for synthesis of methyl 4-((1-phenyl-1H-pyrazolo[3,4-d]pyrimidin-4-yl)amino)benzoate (5)

The desired compound 5 was obtained by refluxing (2.31 g, 0.01 mol) of 4-chloro-1-phenyl-1*H*-pyrazolo[3,4-d]pyrimidine (4) and methyl 4-aminobenzoate (1.51 gm, 0.01 mol) in acetonitrile (20 ml).. After allowing the mixture to cool, the separated solid from the ethanol was filtered and recrystallized to afford the corresponding methyl ester **5**.

Yield, 82%; m.p. 246-8°C; IR_{vmax} (cm^{-1}): 1689 (C=O), 2952 (CH aliphatic), 3042 (CH aromatic), 3341 (NH); ^{1}H NMR (400 MHz, DMSO-d_6): 10.77 (s, 1H, NH, D_2O exchangeable), 8.80 (s, 1H, CH of pyrimidine), 8.60 (s, 1H, CH of pyrazole), 8.18 (d, 2H, H-2, H-6 of C_6H_5), 8.12 (d, 2H, C-3 and C-5 of C_6H_4), 7.96 (d, 2H, C-2 and C-6 of C_6H_4), 7.53-7.57 (m, 2H, C-3 and C-5 of C_6H_5), 7.34-7.38 (m, 1H, C-4 of C_6H_5), 3.82 (s, 3H, CH_3); ^{13}CNMR: 197.87, 156.22, 153.24, 143.89, 138.70, 133.94, 131.86, 129.74 (2), 129.66, 127.17, 121.91, 121.54 (2), 120.35 (2), 107.84, 103.21, 26.74; MS (m/z): 199.50 (100 %, base beak), 342.35 (67.89 %), 345.61 (M^+, 27.16 %), 347.89 ($M^+ + 2$, 2.73 %).

2.1.6. General method for synthesis of 4-[(1-Phenyl-1H-pyrazolo[3,4-d]pyrimidin-4-yl)amino]benzo-hydrazide (6).

As per the described protocol, The desired compound (6) was obtained by refluxing a mixture of hydrazine hydrate (80%, 20 ml) and methyl 4-((1-phenyl-1*H*-pyrazolo[3,4-d]pyrimidin-4-yl)amino)benzoate (5) (3.45 g, 0.01 mol) in absolute ethanol (50 ml) for 8 hours, cooling, and collecting the crude product through filtration, drying, and recrystallization using ethanol.

Yield, 82% as reported; m.p. 260–2 ◦C as recorded; ^{13}C NMR: 158.67, 153.02, 152.61, 148.99, 139.48, 138.63, 138.11, 136.73, 130.00, 129.85, 128.17, 127.69, 124.12 (2), 95.94, 104.48, 122.64 (2),

2.1.7. General method for synthesis of targeted compound N-cyclohexyl-2-(4-((1-phenyl-1H-pyrazolo[3,4-d]pyrimidin-4-yl)amino)benzoyl)hydrazine-1-carboxamide (7)

Refluxing for five hours a mixture of the cyclohexyl isocyanate (1.25 g, 0.001 mol) and acid hydrazide (6) (0.35 g, 0.001 mol) in absolute ethanol (25 ml). The mixture was then cooled and the formed precipitate is filtered and recrystallized to give the desired compound (7).

Yield, 65%; m.p. 287-9^{o}C; IR$_{vmax}$ (cm^{-1}): 1658 (2C=O), 2965 (CH aliphatic), 3040 (CH aromatic), 3428, 3280, 3100 (4NH),; ^{1}H NMR (400 MHz, DMSO-d$_6$): 12.08 (s, 2H, 2NH, D_2O exchangeable), 8.43 (s, 1H, CH of pyrimidine), 8.23 (s, 1H, CH of pyrazole), 8.01 (s, 1H, NH, D_2O exchangeable), 7.92 (d, 2H, H-2 and H-6 of C_6H_5), 7.53-7.62 (m, 5H, H-3, H-4, H-5 of C_6H_5 and H-2, H-6 of C_6H_4), 7.37-7.45 (d, 2H, H-3 and H-5 of C_6H_4), 7.00 (s, 1H, NH-cyclohexyl, D_2O exchangeable), 3.40-3.45 (m, 1H, C-1 of cyclohexyl), 1.62-185 (m, 4H, C-2 and C-6 of cyclohexyl), 1.50 (m, 2H, C-4 of cyclohexyl), 1.23 (m, 4H, C-3 and C-5 of cyclohexyl); ^{13}CNMR: 180.86, 158.80, 152.91, 152.55, 148.95, 139.40, 137.91, 136.69, 130.06, 129.89 (2), 128.30, 127.79, 124.12 (2), 122.66 (2), 104.36, 95.67, 53.31, 31.99 (2), 25.39, 24.98 (2); MS (m/z): 320.38 (29.89 %), 343.43 (100 %, base beak), 459.18 (11.67 %), 470.59 (M^+, 11.68 %).

2.2. Molecular Docking

The modeling portion's goal is to explain the in vitro anticancer action on a molecular level. Since the EGFR and VEGFR enzymes are the focus of our design method, we performed molecular docking tests on typical targeted compound 7 with the crystal structures for VEGFR and EGFR (PDB codes: 4ASD and 3W2O) [23,31] respectively.

2.2.1. Studies using molecular docking Preparing Ligands

Studies using molecular docking identify the relationships between the targeted protein and the chosen molecule. These investigations were carried out with Molsoft and AutoDock Vina. Molsoft was used for preparation of protein required for docking studies. AutoDock Vina is used as visualizer for docking poses and orientations which used for molecular dynamic simulations. ChemDraw Ultra 8 software was used to create the ligands, and the Merck Molecular Field (MMFF) was used to optimize them so they would attach to the protein-binding site with the least amount of free energy possible [32].

2.2.2. Protein preparation

To obtain comprehensive in silico evaluations of the substances and guarantee strong interaction with the protein structures, the numerous intended screening compounds were docked against certain recognized commercial standards. PDB (Co-crystallized ligand: Sorafenib, PDB: 4ASD) was retrieved from RCSB VEGFR. These protein structures were prepared and enhanced using UCSF Chimera and the AMBER Force Field. Water molecules and the co-crystallized ligand were eliminated. Kollmann, missing residues, polar hydrogens, and charges of the AD4 type were all inserted. The protein was saved in PDBQT format with the binding pocket indicated [33].

Using Molsoft and Auto dock vina, in-silico docking was also done. The docking of low-energy stable conformers was chosen. Electrostatic interactions, hydrophobic interactions, and hydrogen bond interactions were examined after docking. Protein-ligand complexes' binding affinities were calculated and compared to those of common medications. The compounds' binding affinities were computed. Each PDB structure's co-crystallized ligand was removed and redocked into its active binding site in order to validate the docking procedure. Interaction of co-crystallized ligands and its PDB sum interaction were evaluated after re-docking [34-36].

3. Results and discussion

3.1. Chemistry

The targeted compound 7 was obtained according to steps followed in scheme 1. Synthesis was started by condensation of triethylorthoformate and ethyl 2-cyanoacetate in the presence of acetic anhydride to afford ethyl 2-cyano-3-ethoxyacrylate (1) which underwent further cyclization reaction with phenylhydrazine [37] to afford ethyl 5-amino-1-phenyl-1H-pyrazole-4-

carboxylate (2). Consequent reflux of 2 with formamide afforded 1-phenyl-1,5-dihydro-4*H*-pyrazolo[3,4-*d*] pyrimidin-4-one (3) [27]. Chlorination of (3) by heating with $POCl_3$ afforded the intermediate 4-chloro-1-phenyl-1*H*-pyrazolo[3,4-d]pyrimidine (4) [38] that reacted with methyl 4-aminobenzoate to produce the corresponding methyl 4-((1-phenyl-1*H*-pyrazolo[3,4-*d*]pyrimidin-4-yl)amino)benzoate (5). Refluxing of the methyl ester derivative 5 with hydrazine hydrate resulted in the corresponding hydrazide 6. Condensation of the hydrazide 6 with cyclohexyl isocyanate afforded the corresponding semicarbazide derivative *N*-cyclohexyl-2-(4-((1-phenyl-1*H*-pyrazolo[3,4-*d*]-pyrimidin-4-yl)amino)benzoyl)hydrazine-1-carboxamide (7) (Schemes 1).

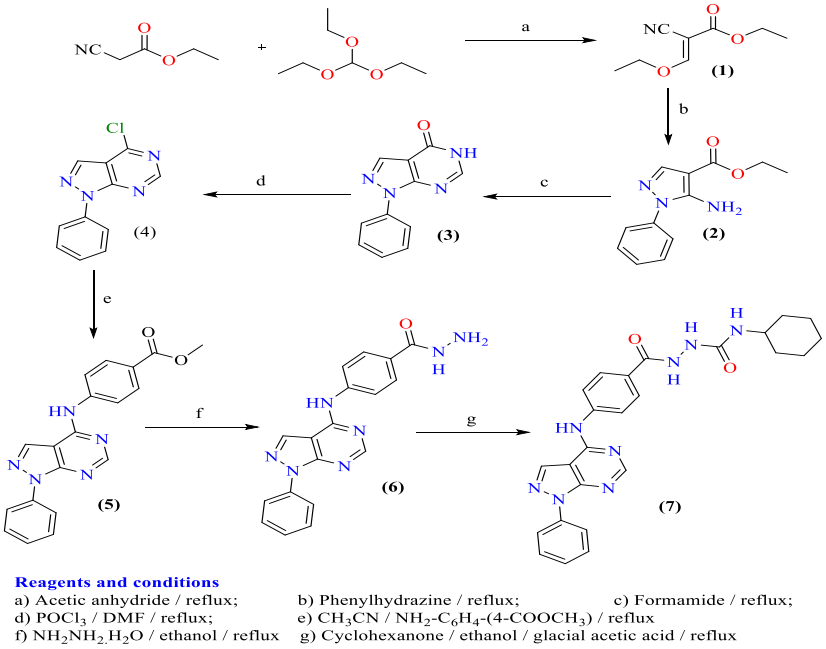

Scheme 1: Synthetic scheme for preparation of the target compounds 1-7

3.2. Rationale and structure-based design

Protecting the structural integrity of the target compounds allowed the pair to retain their critical pharmacophoric configuration, which includes EGFR and VEGFR-2 inhibitors.

There are many VEGFR-2 inhibitors, Sorafenib is one of them and has four essential characteristics [39,40]; (i) a flat hetero aromatic ring that is compatible with the adenosine triphosphate (ATP)-binding site [41]. (ii) A central hydrophobic linker [42]. (iii) A spacer that has HBD and/or HBA which maintains the cohesion with the two important residues (Glu885 and Asp1046). (iv) The allosteric hydrophobic pocket is completely engulfed by the final hydrophobic component [43] (Fig. 1).

Bioisosteric modification techniques were used to carry out our master plan for the molecular design justification on (Sorafenib) at four different locations, as shown in Fig. 1.

The fundamental concept is to mimic VEGFR-2 inhibitors by incorporating phenyl rings into the pyrazolopyrimidine scaffold at position 1 and retaining the ATP-domain. Phemyl amino linkers are inserted into the linker region as the second alteration. The third adjustment is to adopt the gate area by using different spacers. Because of their elongated structure, which enables them to pass outside the gate area and inhabit the nearby allosteric hydrophobic cavity, our final compounds can be classified as type II inhibitors. The fourth alteration involves binding distinctive hydrophobic cyclohexyl moiety to the allosteric hydrophobic pocket. These four elements were used in our final products to replace the four pharmacophoric portions of sorafenib. Also, there are many EGFR inhibitors for example Erlotinib. Erlotinib is guaranteed to undergo structural modification at each of the four locations shown in Fig. 4 by the aforementioned derivations.

The modulation at the headmost position made use of the biological isostere idea because they were EGFR inhibitors. The hetero aromatic quinazoline was substituted with pyrazolopyrimidine, which is resting in the adenine binding groove. The second portion (lipophilic head) of the phenyl ring was replaced with cyclohexyl one. The NH linker was used in the third part. To enhance the

binding characteristics with the EGFR receptor, additional semicarbazide spacer was also employed. The phenyl ring was attached at position 1 of the pyrazolopyrimidine nucleus so that it could reside in the hydrophobic socket II of the ATP binding region which occupied by the hydrophobic tail (2- methoxyethoxy groups).

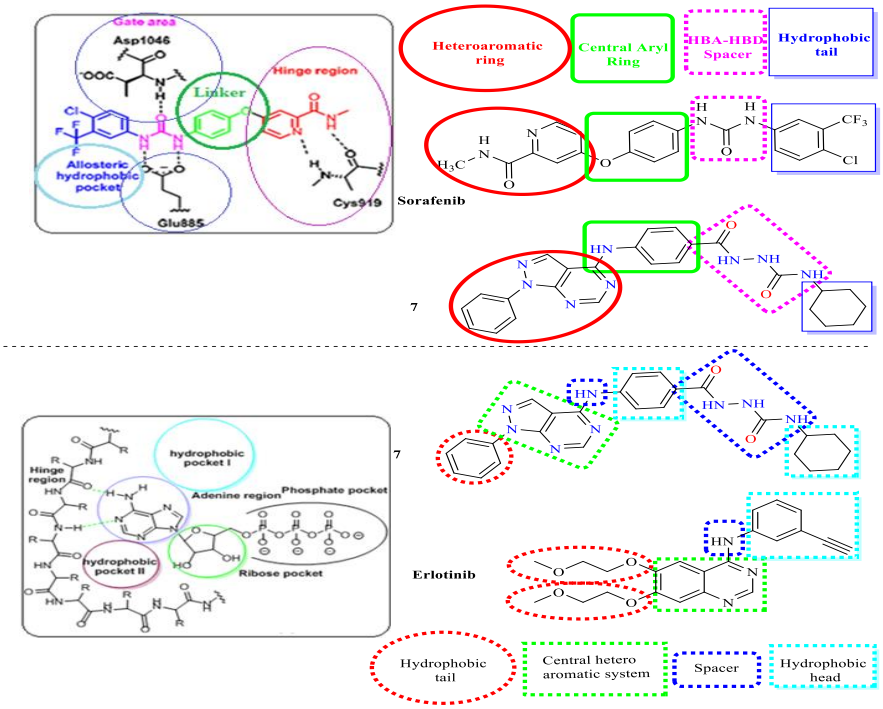

Fig 1: Structural similarity of compound 7 against Sorafinib (VEGFR-2 inhibitor) and Erlotinib (EGFR-TK inhibitor)

Early SAR research focused on the effects of substituting phenyl and 1-phenylpyrazolopyrimidine moieties for the two methoxyethoxy group moieties in erlotinib and the pyridine ring in sorafenib, respectively. It also focused on the effects of switching to lengthy spacers for the urea and amino linkers in sorafenib and erlotinib respectively. To assess their impact on the anticancer activity, cyclohexyl substituent with lipophilic and electron donating properties was applied to the phenyl tail of our molecules through long semicarbazide linker. This compound showed variable anticancer activity compared to sorafenib and erlotinib against four tested cell lines (A549, MCF-7, HepG2 and HCT116).

3.3. ADMET profile

In silico prediction of ADMET profile was carried out online using the following link https://biosig.lab.uq.edu.au/pkcsm/prediction_single/adme_1724788424.2. Our derivative **7** does not violate any rule of Lipinski's [44]. It is well recognized that CYP3A4, the key enzyme involved in drug metabolism, could be suppressed by erlotinib, sorafenib, and our derivative. In addition it has excellent GIT absorption and very low total clearance, which is a key factor in setting dose intervals, was used to predict elimination. It showed prolonged half-life and longer dose intervals compared to erlotinib and sorafenib. The final analyzed factor for the ADMET profile is toxicity. As shown in **Table 1**, Sorafenib, Erlotinib, and our compound showed unfavorable hepatotoxic side effects. The acute toxic dose of **7** is higher than those of sorafenib and erlotinib.

Table 1: ADMET profile of 7, Sorafenib and Erlotinib;

Parameter	7	Soraf.eni	Erlotinib
Physicochemical properties			
Molecular Weight	470.537	464.831	393.443
LogP	3.8358	5.5497	3.4051
Rotatable Bonds	5	5	10
Acceptors	7	4	7
Donors	4	3	1
Surface Area	201.680	185.111	169.532
Absorption			
Human Intest. absorption	80.529	89.043	94.58
Distribution			
Permeability to CNS	-2.562	-2.007	-3.216
Metabolism			
CYP3A4 substrate	+	+	+
Inhibition of CYP3A4	+	+	+
Excretion			
Clearance	0.329	-0.219	0.702
Toxicity			
Human Max. tolerated dose	0.679	0.549	0.839
Acute Toxic activity (LD_{50})	3.176	2.538	2.393
Chronic Toxic activity (LOAEL)	0.543	1.198	1.37
Hepatotoxic effect	+	+	+

3.4. *Docking targeted compound 7 in 4ASD and 3W2O*

Sorafenib exhibited -99.50 kcal/mol and formed 5 H-bonds with Cys919 (2.51 Å and 2.10 Å), Glu885 (1.77 Å and 2.75 Å) and Asp1046 (1.50 Å). The terminal 3-trifluromethyl-4-chlorophenyl group occupied the hydrophobic channel that outlined by Cys1045, Asp1046, Hie1026, Ile888, Ile892 and Glu885 (Figure 2).

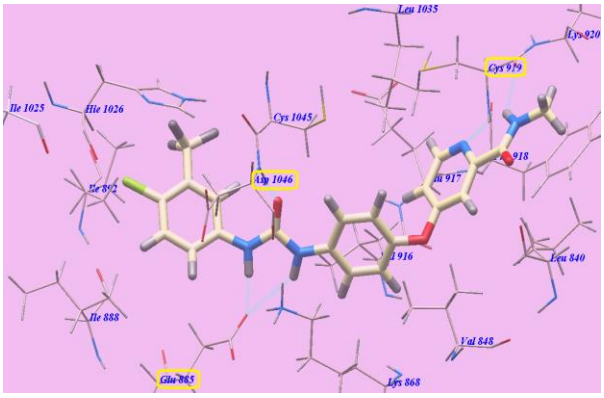

Figure 2: Sorafenib predicted mechanism of binding with 4ASD. Dotted lines represent H-bonds.

Compound **7** showed nearly identical binding mode to that of **Sorafenib.** It showed -114.51 kcal/mol and 4 H-bonds with Cys919 (2.46 Å), Asp1046 (2.29 Å and 2.73 Å) and Glu885 (2.34 Å). The pocket formed by Leu1035, Lys920, Cys919, Phe918, Glu917, Val848 and Leu840 occupied by the 1-phenylpyrazolopyrimidine scaffold. The terminal cyclohexyl tail occupied the hydrophobic channel constructed by Hie1026, Ile892, Ile888 and Glu885 (**Figure 3**).

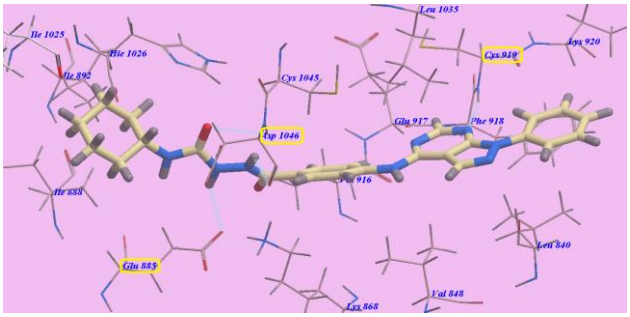

Figure 3: Compound 7 predicted binding mode with 4ASD.

Erlotinib displayed -82.77 kcal/mol and four H-bonds with Cys797 (2.05 Å), Val726 (2.97 Å), Met793 (1.82 Å) and Thr854 (2.99 Å). 3-Ethynylphenyl head occupied the hydrophobic region I, which formed by Met790, Glu791, Glu762, Val726, Ile759, Leu777, Asp855, Thr854, and Phe723. Additionally, the 2-methoxyethoxy tail occupied the hydrophobic area II generated by Leu844, Met793, Pro794, Val845, and Leu718 (Figure 4).

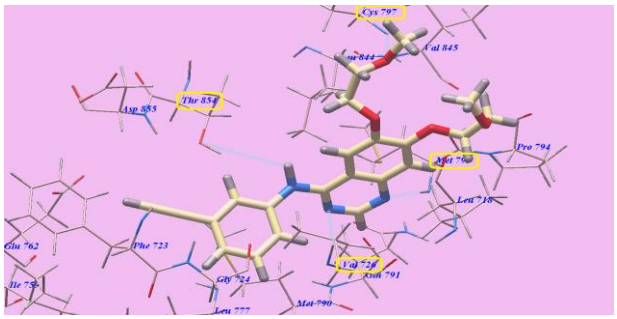

Figure 4: Docking results for Erlotinib with 3W2O.

Compound 7 showed binding orientation that is nearly identical to erlotinib. It displayed -99.25 kcal/mol and 5 H-bonds with Phe723 (2.08 Å and 2.62 Å), Glu762 (2.98 Å), Lys745 (2.97 Å) and Met793 (2.40 Å). 1-Phenylpyrazolopyrimidine occupied the hydrophobic region II, which produced by Met793, Pro794, Cys797, Leu844, Val845, and Leu718. The central phenyl group occupied the hydrophobic region I, which was generated by Leu788, Met790, Thr854, Asp855, and Gly724. Moreover, the extra hydrophobic cyclohexyl ring occupied the hydrophobic region generated by Ile759, Glu758, Phe723, and Glu762 (Figure 5).

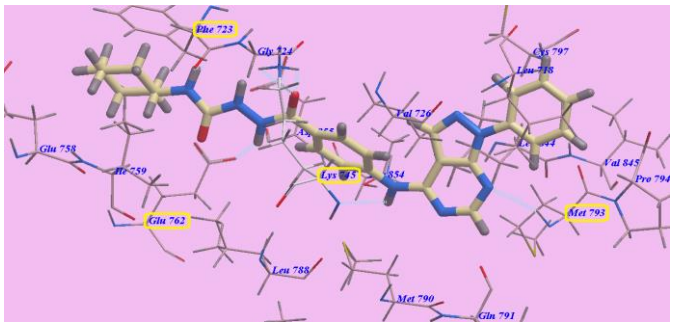

Figure 5: Predicted binding mode for 7 with 3W2O.

3.5. Molecular dynamics simulation

The highly active derivative 7 in the proteins VEGFR-2 and EGFR was simulated using molecular dynamics (MD). By utilizing Amber's MM/GBSA.py script and the trajectory, the receptor-ligand binding energy was calculated [25]. Additionally, the employed as positive controls were sorafenib and erlotinib respectively. With the help of GAFF2 [27] and the force field AMBERff14SB for the protein, ligand force fields were produced [26]. The monitored root mean square deviation (RMSD) validated the studied inhibitor compounds' considerable global stability inside the target's recognized active site throughout the 50 ns all-atom MD runs (Figures 6&7). The given ligands molecular divergences from a defined original/reference structures were estimated using RMSD. The selected MD simulation procedures were valid, and gave a respectable suggestion of the stability of the ligands-target interactions.

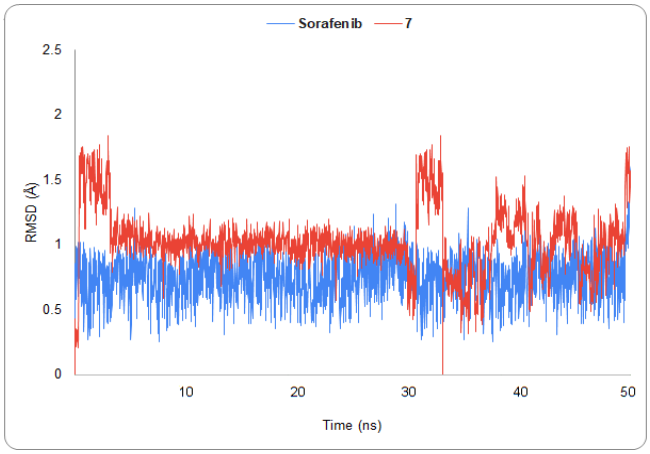

Figure 6: Analysis of VEGFR-2 protein RMSD throughout 50 ns for the ligand-protein complexes

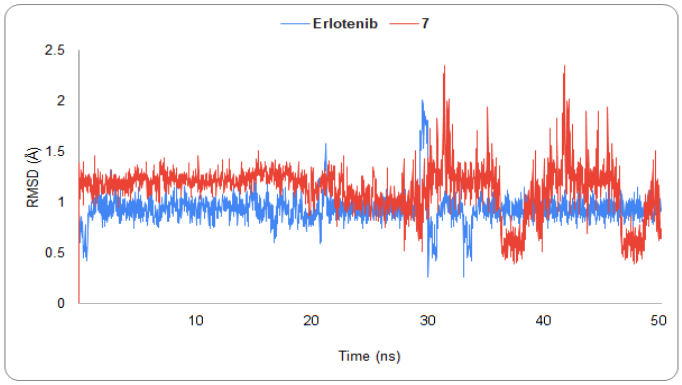

Figure 7: Analysis of EGFR protein RMSD throughout 50 ns for the ligand-protein complexes

3.6. Radiolabeling of N-cyclohexyl-2-hydrazine-1-carboxamide with technetium-99m:

Radiolabeling and in vivo biodistribution with sodium dithionite ($Na_2S_2O_4$) acting as the reducing agent, direct ^{99m}Tc radiolabeling was carried out. In order to attain the best possible radiolabeling, a number of factors influencing the procedure were investigated. Targeted compound amount is (200–1000 µg), Na2S2O4 amount (1–5 mg), pH (2–8), and reaction time is (1–30 min). The tagged compound's in vitro stability was evaluated at room temperature for a day. To calculate the percentages of ^{99m}Tc-targeted complex, free $^{99m}TcO4$- and colloid, ascending paper chromatography (P.C.) was used to analyze radiochemical yields of ^{99m}Tc-targeted complex. One-way ANOVA was utilized to evaluate the differences in the data, with a significance threshold of P 0.05.

3.7. Effect of sodium dithionite content (Reducing agent effect).

In order for ^{99m}Tc to be prepared for complexation with the ligand, $^{99m}TcO4$ is lowered to a condition of reduced oxidation using sodium dithionite. The radiochemical yield of the ^{99m}Tc-targeted pyrazolopyrimidine compound was severely impacted by the 0.5–1 mg of sodium dithionite concentration, as seen in Fig 8. The radiochemical yield at low sodium dithionite (1 mg) was

45.6%. The greatest radiochemical yield of the ^{99m}Tc-targeted molecule (93.4%) was obtained with a concentration of 3 mg after raising the sodium dithionite content to 2 mg. The radiochemical yield of the ^{99m}Tc-targeted molecule declined and the free ^{99m}TcO4−rose at doses greater than 3 mg.

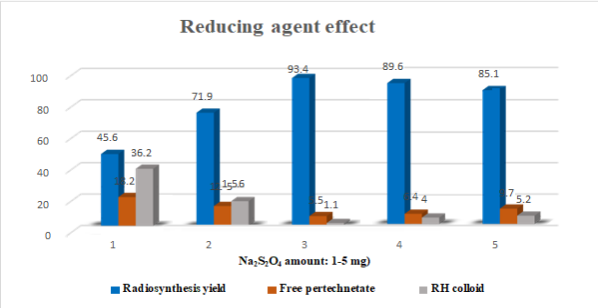

Figure 8: Effect of sodium dithionite content (Reducing agent effect)

3.8. *Effect of reaction time*

The ^{99m}Tc-pyrazolopyrimidine combination could not form in the brief reaction period of 1 minute, resulting in a low labeling yield of 19.1%. The radiochemical yield increased to 30.7% after increasing the reaction time to 5 minutes. The yield massively increased to 93.4% after increasing the reaction time to 10 minutes, and stayed constant after increasing the reaction time to 30 minutes (Fig 9.).

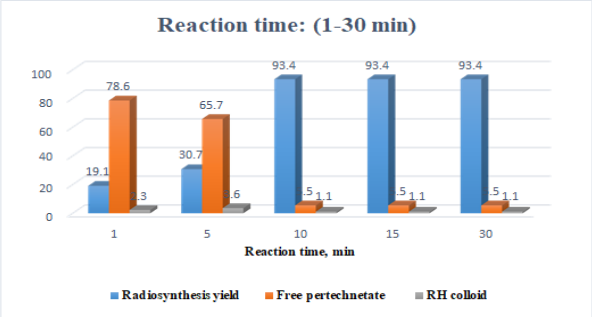

Figure 9: Effect of reaction time

3.9. Effect of complexing agent

A solution with a concentration of 1 mg/ml 0.1–1 µg was used in studying the effect of the targeted compound content in the range of 200–1000 µL (Fig. 10). The radiochemical yield of the 200 µL pyrazolopyrimidine targeted compound was low at 22.3% because there was not enough of the compound to complex all of the reduced technetium-99m. By raising the targeted compound amount to 400 µL, the radiochemical yield increased to 54.5%. Raising the compound to 600 µL resulted in the greatest yield of radiochemical ^{99m}Tc-targeted compound (93.4%). Then, as the amount was increased over 600 µL, the radiochemical yield decreased somewhat.

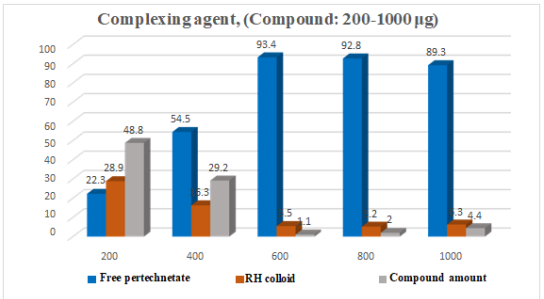

Figure 10: Effect of complexing agent

3.10. Effect of PH

The ^{99m}Tc-pyrazolopyrimidine targeted compound's labeling yield began at a low percentage (28.4%) when using a low pH of 2, but it increased as the reaction medium's pH increased (Fig. 11) to 51.2% at a PH of 5, and it reached its maximum yield (93.4%) at pH 6, at which the pyrazolopyrimidine combined with all of the reduced technetium. The labeling yield dropped to 73.4% at a pH of 7 and 66.9% at a pH of 8 with additional pH increases. This is because high pH levels cause Na2S2O4 to precipitate easily, and in an alkaline media, high pH levels also encourage the production of insoluble decreased hydrolyzed ^{99m}Tc colloid and free ^{99m}TcO4 [45-47].

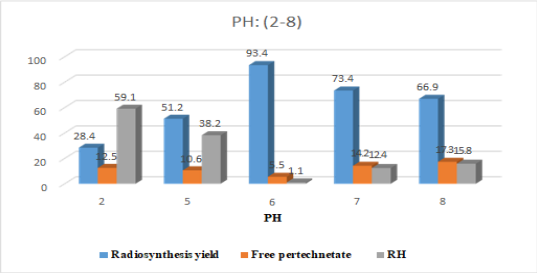

Figure 11: Effect of PH

3.11. Different biodistribution of radio targeted compound on excretory organs

In tumor-bearing mice model (a group of 30 female mice): *in vivo* cancer targeting ability research of ^{99m}Tc- targeted chemical Figs. 12&13 depicts the *in vivo* biodistribution of a drug that targets ^{99m}Tc in tumor-bearing animals at various time points. At all time periods, the uptake of the affected muscle (T. muscle) was larger than that of the healthy muscle Fig. 14. High amounts of radioactivity in the liver, gut, and kidneys suggest that the hepatobiliary and urinary routes are the means by which the ^{99m}Tc-targeted molecule is excreted. The ratio of target to non-target (T/NT) reveals the molecule's selectivity and capacity to target a particular organ or sick tissue [48,49]. When the T/NT value is greater than 1.5, the molecule is considered selective, and the selectivity increases as the T/NT value raises. In this study, the sick left thigh muscle in the mouse's served as the target, and the healthy muscle in the mouse's other thigh served as the non-target [50].

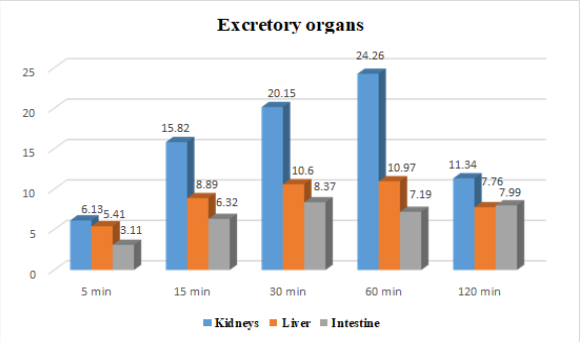

Figure 12: Biodistribution of radio targeted compound on excretory organs

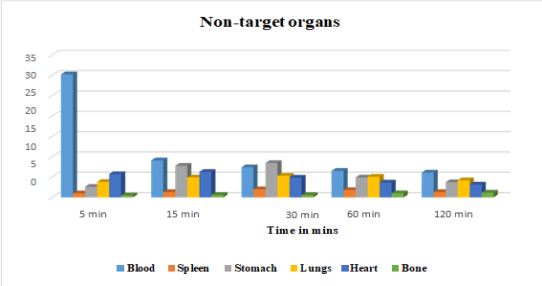

Figure 13: Biodistribution of radio targeted compound on non-target organs

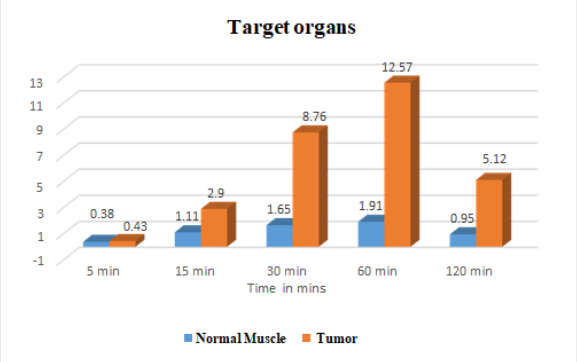

Figure 14: The uptake of the affected muscle and healthy normal muscle

As illustrated in Fig. 15, the ratio of target to non-target (affected muscle/normal muscle; T/NT) was consistently greater than 1 and peaked at 60 minutes after injection (T/NT = 6.58).

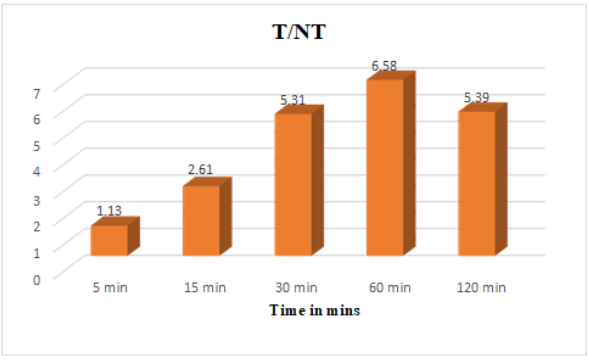

Figure 15: the ratio of target to non-target (affected muscle/normal muscle; T/NT)

4. Conclusion

This study intended to develop a pyrazolopyrimidine derivative as more effective novel anticancer agent. The synthesized compound 7 was labeled with ^{99m}Tc at great radio-synthetic yield then in-vivo studied after presenting high accumulation at tumor sites. Consequently it was discovered that the synthesized compound might be radiolabeled with gamma emitter ^{99m}Tc as a prospective imaging agent for tumor sites and can be used as a potent anticancer agent after additional preclinical studies.

Acknowledgment

The research for this publication was funded by grant (46045) from the Science, Technology, and Innovation Funding Authority (STDF).

Conflict of interest: No

References

1. C.J. Cabasag, P.J. Fagan, J. Ferlay, J. Vignat, M. Laversanne, L. Liu, M.A. van der Aa, F. Bray, I. Soerjomataram, Int. J. Cancer. 151 (2022) 1535-1541.
2. P.S. Hegde, D.S Chen, Immunity 52 (2020) 17–35.
3. N. Vasan, J. Baselga, D.M. Hyman, Nature 575 (2019) 299–309. https://doi.org/10.1038/s41586-019-1730-1.
4. K. Asgaonkar, S. Tanksali, K. Abhang, A. Sagar, Journal of the Indian Chemical Society 100 (2023) 100803, https://doi.org/10.1016/j.jics.2022.100803.
5. Z. Schrank, G. Chhabra, L. Lin, T. Iderzorig, C. Osude, N. Khan, A. Kuckovic, S. Singh, R.J. Miller, N. Puri, Cancers (Basel) 10 (2018) 224. doi: 10.3390/cancers10070224.
6. C.K. Thammaiah, S. Jayaram, Noncoding RNA Res. 1 (2016) 77-82. doi: 10.1016/j.ncrna.2016.10.003.

7. P.R. Sankar, A.B. Sailu, M.M. Eswarudu, M.N. Satya, P. Sreeja, P. Roja, Sk. Rijwana Sankar, J. Pharm. Sci. & Res. 13 (2021) 313-318.
8. F. Broekman, E. Giovannetti, G.J. Peters, World J Clin. Oncol. 2 (2011) 80-93. doi: 10.5306/wjco.v2.i2.80.
9. M.A. Abdelgawad, N.A.A. Elkanzi, A.A. Nayl, A. Musa, Nasser H. Alotaibi, W.A.A. Arafa, S.M. Gomha, R.B. Bakr, Arabian Journal of Chemistry, 15 (2022), 103781, https://doi.org/10.1016/j.arabjc.2022.103781.
10. J. Fares, M.Y. Fares, H.H. Khachfe, H.A. Salhab, Y. Fares Signal Transduct Target Ther. 5 (2020) 28. doi: 10.1038/s41392-020-0134-x.
11. G. Follain, D. Herrmann, S. Harlepp, V. Hyenne, N. Osmani, S.C. Warren, P. Timpson, J.G. Goetz . Nat Rev Cancer. 20 (2020) 107-124. doi: 10.1038/s41568-019-0221-x.
12. T.B. Steinbichler, D. Savic, J. Dudás, I. Kvitsaridze, S. Skvortsov, H. Riechelmann, I.-I. Skvortsova, 60 (2020) 148-156, https://doi.org/10.1016/j.semcancer.2019.09.007.
13. D. Alferez, R.W. Wilkinson, J. Watkins, R. Poulsom, N. Mandir, S.R. Wedge, I.T. Pyrah, N.R. Smith, L. Jackson, A.J. Ryan, R.A. Goodlad, Mol Cancer Ther. 7 (2008) 590-598. doi: 10.1158/1535-7163.MCT-07-0433.
14. A.E. Mghwary, E.M. Gedawy, A.M. Kamal, S.M. Abuel-Maaty, J Enzyme Inhib Med Chem. 34 (2019) 838-852. doi: 10.1080/14756366.2019.1593160.
15. S.A. Lang, P. Schachtschneider, C. Moser, A. Mori, C. Hackl, A. Gaumann, D. Batt, H.J. Schlitt, E.K. Geissler, O. Stoeltzing, Mol Cancer Ther. 7 (2008) 3509-3518. doi: 10.1158/1535-7163.MCT-08-0373.
16. A.K. Larsen, D. Ouaret, K. El Ouadrani, A. Petitprez, Pharmacol Ther. 131 (2011) 80-90. doi: 10.1016/j.pharmthera.2011.03.012.
17. P.A. Jänne, J.C. Yang, D.W. Kim, D. Planchard, Y. Ohe, S.S. Ramalingam, M.J. Ahn, S.W. Kim, W.C. Su, L. Horn, D. Haggstrom, E. Felip, J.H. Kim, P. Frewer, M. Cantarini, K.H. Brown, P.A. Dickinson, S. Ghiorghiu, M. Ranson, N Engl J Med. 372 (2015) 1689-99. doi: 10.1056/NEJMoa1411817.
18. X. Le, M. Nilsson, J. Goldman, M. Reck, K. Nakagawa, T. Kato, L.P. Ares, B. Frimodt-Moller, K. Wolff, C. Visseren-Grul, J.V. Heymach, E.B. Garon, J Thorac Oncol. 16 (2021) 205-215. doi: 10.1016/j.jtho.2020.10.006.
19. L. Xi, J.Q. Zhang, Z.C. Liu, J.H. Zhang, J.F. Yan, Y. Jin, J. Lin, Org Biomol Chem. 11 (2013) 4367-78. doi: 10.1039/c3ob40368h. Epub 2013 May 28. PMID: 23715382.
20. N.M. Saleh, M.G. El-Gazzar, H.M. Aly, R.A. Othman, Front Chem. 7 (2020) 917. doi: 10.3389/fchem.2019.00917.
21. T. Zhang, H. Lei, X. Chen, Z. Dou, B. Yu, W. Su, W. Wang, X. Jin, T. Katsube, B. Wang, H. Zhang, Q. Li, C. Di, Cell Death Discov. 10 (2024) 16. doi: 10.1038/s41420-023-01778-3.
22. K. Kumar, Molecules. 26 (2021) 6227. doi: 10.3390/molecules26206227.
23. G.M. Morris, R. Huey, W. Lindstrom, M.F. Sanner, R.K. Belew, D.S. Goodsell, A.J. Olson, J Comput Chem. 30 (2009) 2785-2791. doi: 10.1002/jcc.21256.
24. N.A.A.M. Aziz, R.F. George, K. El-Adl, W.R. Mahmoud, Arch. Pharm. 356 (2022) e2200465. https://doi.org/10.1002/ardp.202200465.
25. H. Liu, Y. Jin, H. Ding, Brief Bioinform. 24 (2023) bbad057. doi: 10.1093/bib/bbad057.
26. J.A. Maier, C. Martinez, K. Kasavajhala, L. Wickstrom, K.E. Hauser, C. Simmerling, J Chem Theory Comput. 11 (2015) 3696-3713. doi: 10.1021/acs.jctc.5b00255.
27. J. Wang, R.M. Wolf, J.W. Caldwell, P.A. Kollman, D.A. Case, J Comput Chem. 25 (2004) 1157-1174. doi: 10.1002/jcc.20035.
28. K. Somakala, S. Tariq, M. Amir, Bioorg Chem. 87 (2019) 550-559. doi: 10.1016/j.bioorg.2019.03.037.
29. Z. Wang, N. Wang, S. Han, D. Wang, S. Mo, L. Yu, H. Huang, K. Tsui, J. Shen, J. Chen, PLoS One. 8 (2013) e68566. doi: 10.1371/journal.pone.0068566.
30. Z. Zhao, H. Wu, L. Wang, Y. Liu, S. Knapp, Q. Liu, N.S. Gray, ACS Chem Biol. 9 (2014) 1230-1241. doi: 10.1021/cb500129t.
31. N.A.A.M. Aziz, R.F. George, K. El-Adl, W.R. Mahmoud, Arch. Pharm. 356 (2022), e2200465. https://doi.org/10.1002/ardp.202200465.

32. L.D. Mendelsohn, Journal of Chemical Information and Computer Sciences, 44 (2004) 2225-2226.
33. W.K.B. Chan, K.M. Olson, J.W. Wotring, J.Z. Sexton, H.A. Carlson, J.R. Traynor, Sci Rep 12 (2022) 5320, https://doi.org/10.1038/s41598-022-08320-y.
34. S. Kumar, P. Kashyap, S. Chowdhury, S. Kumar, A. Panwar, A. Kumar, Phytomedicine. 85 (2021) 153317. doi: 10.1016/j.phymed.2020.153317.
35. O. Trott, A.J. Olson, J. Comput. Chem. 31 (2010) 455-461. doi: 10.1002/jcc.21334.
36. M.D. Hanwell, D.E. Curtis, D.C. Lonie, T. Vandermeersch, E. Zurek, G.R. Hutchison, J Cheminform. 4 (2012) 17. doi: 10.1186/1758-2946-4-17.
37. A.A. Gaber, A.M. El-Morsy, F.F. Sherbiny, A.H. Bayoumi, K.M. El-Gamal, K. El-Adl, A.A. Al-Karmalawy, R.R. Ezz Eldin, M.A. Saleh, H.S. Abulkhair, Arch Pharm (Weinheim) (2021) e2100258. doi: 10.1002/ardp.202100258.
38. R.B. Bakr, E.K.A. Abdelall, M.K. Abdel-Hamid, M.M. Kandeel, Bull. Pharm. Sci., Assiut Univ. 35 (2012) 27-42. https://api.semanticscholar.org/CorpusID:220743673.
39. Q.Q. Xie, H.Z. Xie, J.X. Ren, L.L. Li, S.Y. J Mol Graph Model. 27 (2009) 751-758. doi: 10.1016/j.jmgm.2008.11.008.
40. K. Lee, K.W. Jeong, Y. Lee, J.Y. Song, M.S. Kim, G.S. Lee, Y. Kim, Eur J Med Chem. 45 (2010) 5420-5427. doi: 10.1016/j.ejmech.2010.09.002.
41. V.A. Machado, D. Peixoto, R. Costa, H.J. Froufe, R.C. Calhelha, R.M. Abreu, I.C. Ferreira, R. Soares, M.J. Queiroz, Bioorg Med Chem. 23 (2015) 6497-6509. doi: 10.1016/j.bmc.2015.08.010.
42. J. Dietrich, C. Hulme, L.H. Hurley, Bioorg. Med. Chem. 18 (2010) 5738-5748.
43. D. Adel, K. El-Adl, T. Nasr, T.M. Sakr, W. Zaghary, Journal of Molecular Structure, 1291 (2023) 136047, https://doi.org/10.1016/j.molstruc.2023.136047.
44. C.A. Lipinski, F. Lombardo, B.W. Dominy, P.J. Feeney, Adv. Drug Deliv. Rev., 23 (1997) 3-25. https://doi.org/10.1016/S0169-409X(96)00423-1.
45. TM Sakr, MA Khedr, HM Rashed, ME. Mohamed, Molecules. 23 (2018) 496. doi: 10.3390/molecules23020496.
46. J.P. Huberty, R.S. Hattner, M.R. Powell, Journal of Nuclear Medicine, 15 (1974) 124-126. https://api.semanticscholar.org/CorpusID:43645775.
47. A. Amin, K. El-Azony, I. Ibrahim, The Official Journal of the International Isotope Society, 52 (2009) 467-472. https://api.semanticscholar.org/CorpusID:97481629.
48. T. Nasr, S. Bondock, T.M. Ibrahim, W. Fayad, A.B. Ibrahim, N.A. AbdelAziz, T.M. Sakr, Bioorg. Med. Chem. 28 (2020) 115444, https://doi.org/10.1016/j.bmc.2020.115444.
49. K.O. Mohamed, Y.M. Nissan, A.A. El-Malah, W.A. Ahmed, D.M. Ibrahim, T.M. Sakr, M.A. Motaleb, European Journal of Medicinal Chemistry, 135 (2017) 424-433, https://doi.org/10.1016/j.ejmech.2017.04.069.
50. A.B. Ibrahim, T.M. Sakr, O.M.A. Khoweys, M.A. Motaleb, A. Abd El-Bary, M.T. El-kolaly, Journal of Radioanalytical and Nuclear Chemistry, 303 (2014) 967-975, https://api.semanticscholar.org/CorpusID:95262072.